Oncogene (2015) **34,** 5163–5174

www.nature.com/onc

ORIGINAL ARTICLE

TM9SF4 is a novel V-ATPase-interacting protein that modulates tumor pH alterations associated with drug resistance and invasiveness of colon cancer cells

F Lozupone[1], M Borghi[2], F Marzoli[1], T Azzarito[1], P Matarrese[1], E Iessi[1], G Venturi[1], S Meschini[3], A Canitano[1], R Bona[1], A Cara[1] and S Fais[1]

An inverted pH gradient across the cell membranes is a typical feature of malignant cancer cells that are characterized by extracellular acidosis and cytosol alkalization. These dysregulations are able to create a unique milieu that favors tumor progression, metastasis and chemo/immune-resistance traits of solid tumors. A key event mediating tumor cell pH alterations is an aberrant activation of ion channels and proton pumps such as (H+)-vacuolar-ATPase (V-ATPase). TM9SF4 is a poorly characterized transmembrane protein that we have recently shown to be related to cannibal behavior of metastatic melanoma cells. Here, we demonstrate that TM9SF4 represents a novel V-ATPase-associated protein involved in V-ATPase activation. We have observed in HCT116 and SW480 colon cancer cell lines that TM9SF4 interacts with the ATP6V1H subunit of the V-ATPase V1 sector. Suppression of TM9SF4 with small interfering RNAs strongly reduces assembly of V-ATPase V0/V1 sectors, thus reversing tumor pH gradient with a decrease of cytosolic pH, alkalization of intracellular vesicles and a reduction of extracellular acidity. Such effects are associated with a significant inhibition of the invasive behavior of colon cancer cells and with an increased sensitivity to the cytotoxic effects of 5-fluorouracil. Our study shows for the first time the important role of TM9SF4 in the aberrant constitutive activation of the V-ATPase, and the development of a malignant phenotype, supporting the potential use of TM9SF4 as a target for future anticancer therapies.

Oncogene (2015) **34,** 5163–5174; doi:10.1038/onc.2014.437; published online 9 February 2015

INTRODUCTION

A common modification of malignant cancer cells is the shift in energy metabolism from oxidative phosphorylation to aerobic glycolysis, that is, the 'Warburg effect'. Taken together with high metabolic rates and the poor tissue perfusion, these changes result in extracellular acidosis and intracellular alkalization.[1–3] These pH alterations favor cell proliferation and drug resistance and contribute to metastasis progression, by increasing the migratory and invasive capacity.[4–9]

A key event mediating tumor cell pH alterations is carried out by the activation of proton pumps such as (H+)-vacuolar-ATPase (V-ATPase), which mediates the pumping of H^+ into the lumen of acidic vacuoles and/or into the extracellular environment. This protein consists of a multisubunit complex composed of a cytosolic V1 catalytic domain, responsible for ATP hydrolysis and a transmembranous V0 integral domain that provides the proton channel.[10–13] Recently, it has been shown that the expression of this proton pump is upregulated in several cancers, including colon cancer, even though its role in the latter remains poorly characterized.[14–17]

TM9SF4 is a transmembrane protein belonging to the transmembrane-9 superfamily (TM9SF), which is a well-defined family of proteins characterized by a large hydrophilic N-terminal domain followed by nine transmembrane domains.[18] Although little is known about their function, these proteins have been implicated in adhesion, phagocytosis and innate immunity. Recently, TM9SF1 has been identified as an autophagy-regulating protein[19] and reported to be differentially expressed in urinary bladder cancer cells,[20] while the *TM9SF3* gene has been shown to be upregulated in paclitaxel-resistant breast cancer cell lines and its overexpression has been related with poor gastric cancer patients outcome.[21,22] We have recently reported that TM9SF4, whereas undetectable in healthy skin, is overexpressed in melanoma cells, where it is associated with cannibalism (a phenomenon related with poor prognosis in many tumors), and intracellular pH regulation, contributing to the establishment of the reverse pH gradient status of cancer cells.[23] TM9SF4 overexpression has also been found in acute myeloid leukemia and myelodysplastic syndromes, due to a 3–10 fold amplification of a chromosome 20 fragment (20q11.21) bearing the entire *TM9SF4* gene.[24]

In the present study, we show that TM9SF4 interacts with V-ATPase in colon cancer cells, regulating V-ATPase assembly and activation, thus having an important role in resistance to 5-fluorouracil (5-FU) and in the invasive cells phenotype.

RESULTS

TM9SF4 colocalizes with V-ATPase in colon cancer cells

We first analyzed the TM9SF4 secondary structure by TopPred,[25] observing a marked similarity between TM9SF4 and the structure of the ATP6V0A2 subunit (one of the four isoforms of this subunit) of the V-ATPase V0 transmembrane section (Figure 1a). Both structures seem to be characterized by a large N-terminal domain followed by nine putative transmembrane domains. Furthermore, the two proteins also share their subcellular localization, being

[1]Therapeutic Research and Medicines Evaluation Department, Istituto Superiore di Sanità, Rome, Italy; [2]Infectious, Parasitic and Immune-Mediated Diseases Department, Istituto Superiore di Sanità, Rome, Italy and [3]Technology and Health Department, Istituto Superiore di Sanità, Rome, Italy. Correspondence: Dr F Lozupone, Department of Drug Research and Medicine Evaluation, Istituto Superiore di Sanità , viale Regina Elena 299, 00161 Rome, Italy.
E-mail: francesco.lozupone@iss.it
Received 9 April 2014; revised 4 December 2014; accepted 4 December 2014; published online 9 February 2015

both detectable in endosomal vesicles.[12,23] These findings, along with a common role of TM9SF4 and V-ATPase in regulating intracellular pH, prompted us to hypothesize a molecular interaction between these two proteins. Specifically, we decided to investigate the possible interaction of TM9SF4 and the ATP6V1H subunit of the V1 domain, which is in close proximity of the N terminus of ATP6V0A. The interaction of these two subunits contributes to the regulation of V-ATPase assembly and activation.[13]

As a preliminary step, we verified TM9SF4 and V-ATPase colocalization by laser scanning confocal microscopy. To this aim, scramble-transfected (SCR) and shRNA-mediated TM9SF4-knocked down (TM9SF4-KD) HCT116 cells were stained for TM9SF4 and ATP6V0A2. A significant colocalization of TM9SF4 with ATP6V0A was observed in SCR cells, as indicated by yellow fluorescence in Figure 1b (the merged picture). Conversely, in TM9SF4-KD cells this colocalization was completely lost (Figure 1c), confirming the specificity of the staining. Consistent with our previous results and with the literature on ATP6V0A2,[10,18] no colocalization of TM9SF4 and LAMP1 was observed (Figure 1d). Effective TM9SF4 silencing was verified by quantitative PCR (Supplementary Figure S1A). Similar results were observed using SW480 cells (not shown).

TM9SF4/V-ATPase molecular association in colon cancer cells

Following confocal microscopy results, the TM9SF4/V-ATPase and TM9SF4/LAMP1 molecular interactions were assessed by quantitative fluorescence resonance energy transfer (FRET) analysis of untransfected (not shown), and SCR or TM9SF4-KD HCT116 and SW480 cells (Figure 2a and Supplementary Figure S2, respectively). FRET results were evaluated in terms of FRET efficiency (FE), by using the following algorithm: FE = (FL3DA – FL2DA/*a* – FL4DA/*b*)/FL3DA, where A is the acceptor and D the donor, and where *a* = FL2D/FL3D and *b* = FL4A/FL3A. FE values analyzed, obtained in three independent experiments, clearly indicated a significant molecular interaction between TM9SF4 and the ATP6V1H subunit in both cell lines and, as expected, TM9SF4/ATP6V1H FE values were significantly reduced in TM9SF4-silenced cells ($P < 0.01$)

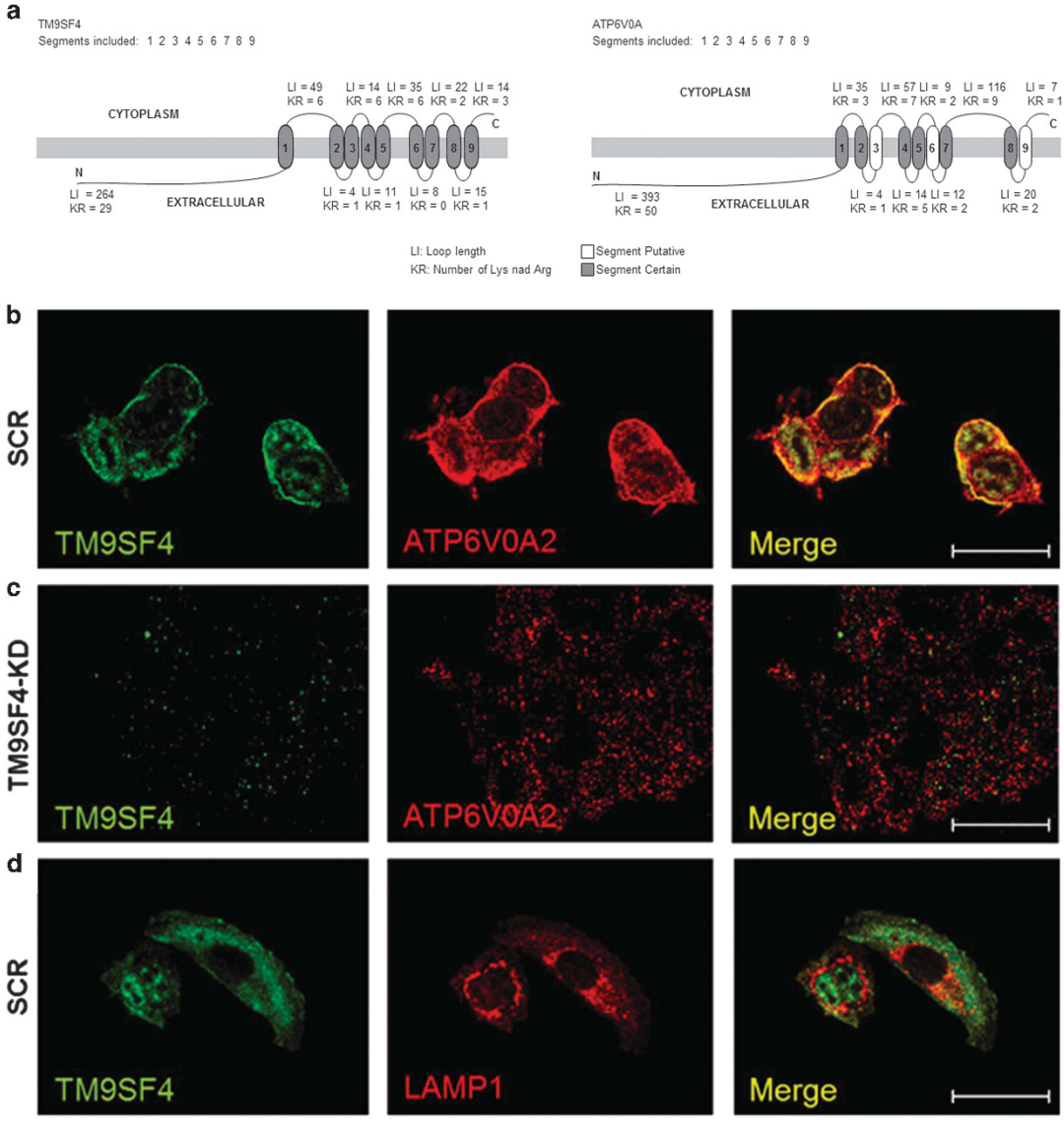

Figure 1. TM9SF4 colocalizes with V-ATPase in colon cancer cells. (**a**) TopPred graphic representation of hydrophobicity values of TM9SF4 and V-ATPase ATP6V0A subunit. Numbers indicate transmembrane domains. Laser scanning confocal microscopy (LSCM) analysis of TM9SF4 (green) and ATP6V0A subunit (red) in: (**b**) SCR and (**c**) TM9SF4-KD cells; (**d**) LSCM analysis of TM9SF4 (green) and LAMP1 (red) in HCT116 cells. Yellow/orange areas in merged picture indicate colocalization Scale bar: 10 μm.

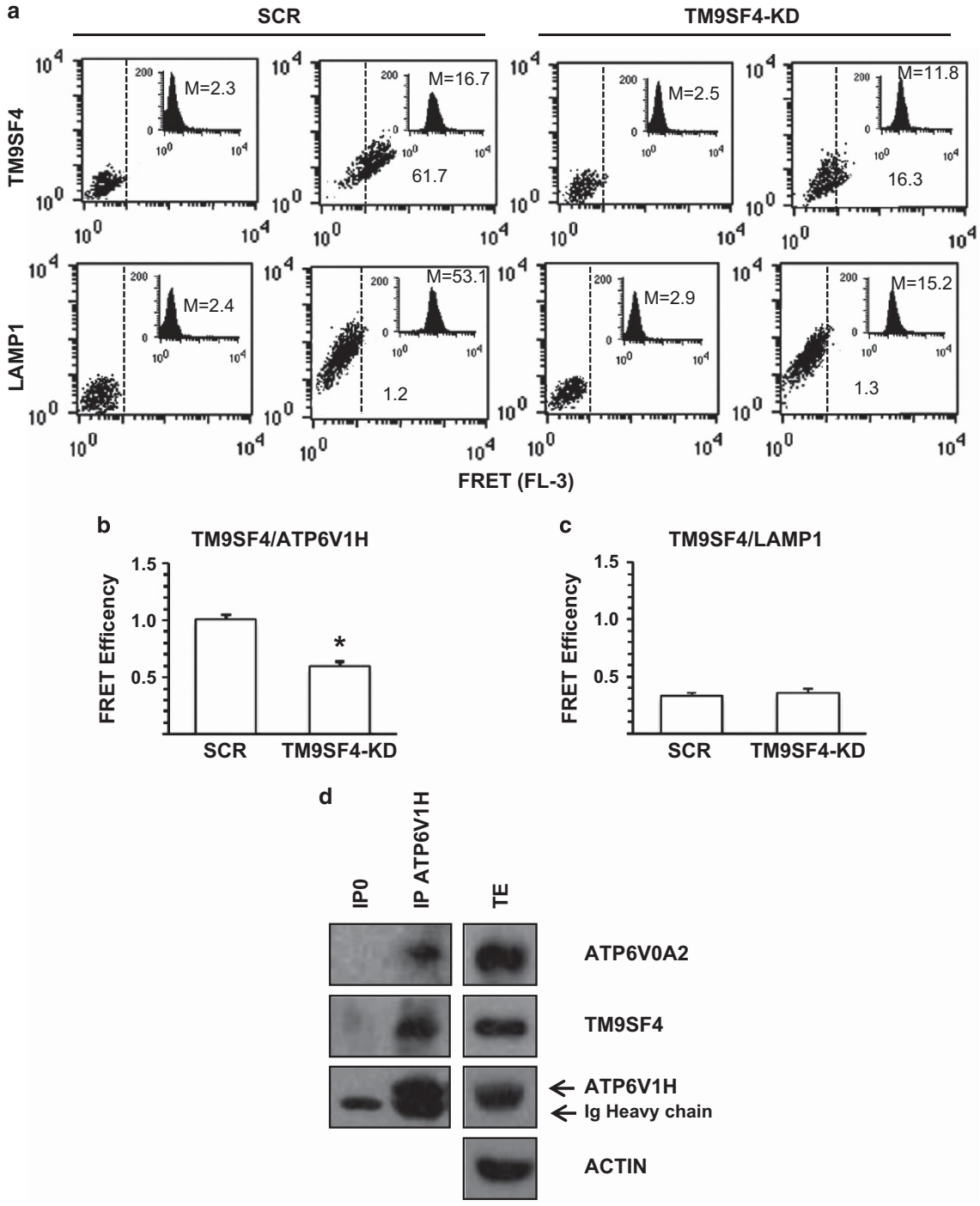

Figure 2. TM9SF4/V-ATPase molecular association in colon cancer cells. (**a**) Flow cytometry analysis of TM9SF4/ATP6V1H or TM9SF4/LAMP1 association by FRET technique in SCR and TM9SF4-KD HCT116 cells. Numbers indicate the percentage of FL3-positive events obtained in one experiment representative of three. Insets represent ATP6V1H (first row) or LAMP1 (second row) intracellular amount in the corresponding sample and is quantitatively expressed by the median fluorescence intensity. (**b**) Bar graphs showing evaluation of FE, according to the Riemann's algorithm, of TM9SF4/ATP6V1H and (**c**) TM9SF4/LAMP1 association. Results shown represent the mean ± s.d. from three independent experiments. $^*P < 0.01$ versus SCR sample. (**d**) Western blot analysis of ATP6V1H immunoprecipitates (IPs) from HCT116 whole extracts immunoblotted for ATP6V0A2 and TM9SF4 detection. IP0: Immunoprecipitation negative control.

(Figure 2b). Consistent with confocal microscopy observations, a negligible association of TM9FS4 with LAMP1 was observed (Figure 2c). Representative FE values of one experiment, calculated following Riemann's algorithm, are shown in Supplementary Table S1.

The same results were obtained by co-immunoprecipitation experiments carried out immunoprecipitating the ATP6V1H subunit from HCT116 total lysates. As shown in Figure 2d, the immunoprecipitated complex contained TM9SF4. The same immunoprecipitates were immunoblotted with an anti-ATP6V1H (as a positive control) and with an antibody to ATP6V0A2 (the other V-ATPase subunit analyzed) to verify the active state of the proton pump.

Altogether, this set of experiments provided strong evidence of the interaction between TM9SF4 and the H subunit of the V1 section of V-ATPase.

TM9SF4 is involved in V-ATPase assembly

Our first set of results showing that TM9SF4 interacts with the V1 section of V-ATPase allowed us to hypothesize that TM9SF4 might modulate V-ATPase holoenzyme assembly and activity. To test this hypothesis, SCR and TM9SF4-KD HCT116 cells were stained for ATP6V0A and ATP6V1H and analyzed by confocal microscopy. As expected, the two subunits strongly colocalized in untransfected (not shown) and in SCR cells (Figure 3a), indicating that in these cells V-ATPase is mainly in its active state. Interestingly, a significant reduction of ATP6V0A/ATP6V1H colocalization was observed in TM9SF4-KD cells (Figure 3b).

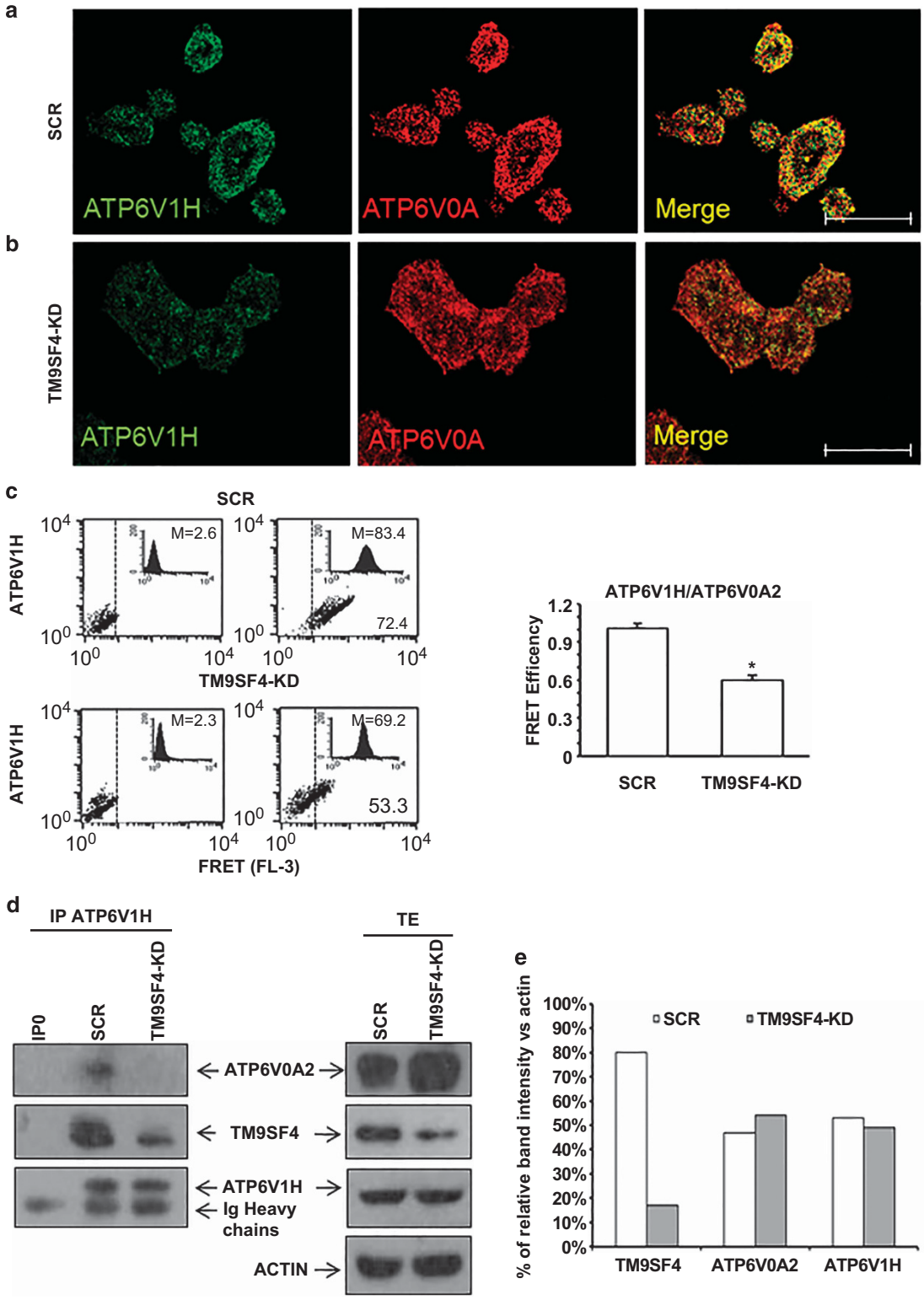

From these results, we next investigated the role of TM9SF4 in V-ATPase assembly. To this aim, FRET experiments were performed to evaluate ATP6V0A/ATP6V1H interaction in SCR and TM9SF4-KD HCT116 and SW480 cells. FE value analysis clearly suggested that TM9SF4 knocking down resulted in a significant reduction ($P < 0.01$) of the association of the two sectors of V-ATPase in both cell lines (Figure 3c and Supplementary Table S1b). Consistent with FRET experiments, blotting the ATP6V1H immunoprecipitates with an anti-ATP6V0A2 antibody, we observed that ATP6V0A was clearly detectable in ATP6V1H immunoprecipitates from SCR whole lysates of both cell lines, while in immunoprecipitates from TM9SF4-KD cells, the signal of the ATP6V0A2 was strongly decreased (Figure 3d). Finally, TM9SF4 inhibition does not influence V-ATPase expression as suggested by western blot densitometric analysis of protein amount of V-ATPase ATP6V1H and ATP6V0A2 subunits in SCR and in TM9SF4-KD HCT116 cells (Figure 3e) and by single fluorescence FRET values of ATP6V0A2 and ATP6V1H expression that did not significantly change when SCR and TM9SF4-KD cells were compared (Supplementary Table S1).

In conclusion, this set of results strongly suggests a TM9SF4 involvement in V-ATPase assembly.

TM9SF4 regulates V-ATPase activity

Next, we tried to verify whether the interaction of TM9SF4 with V-ATPase had any effect on the activity of V-ATPase. To this purpose, we hypothesized that if the binding of TM9SF4 to V-ATPase, contributing to V0/V1 sectors assembly, had a role in the activation of this proton pump, TM9SF4-KD cells should be less sensitive to V-ATPase inhibitors such as bafilomycin (Baf-A1). To verify this hypothesis, we treated SCR or TM9SF4-KD HCT116 and SW480 cells, respectively, with 10 and 70 nM Baf-A1, being SW480 cells less sensitive to the V-ATPase inhibitor (not shown). pH alterations of untreated and Baf-A1-treated SCR and TM9SF4-KD cells were analyzed measuring cytosolic and vesicular pH, by, respectively, using 2′7′-bis (carboxyethyl)-5(6)-carboxyfluorescein (BCECF-AM) and FITC-dextran.[10] Consistent with our previous work, TM9SF4 silencing reverted the tumor cell pH intracellular gradient in both cell lines. In fact, the TM9SF4 knocking down resulted in a significant decrease of the cytosolic pH (pHi) and a consequent alkalization of intracellular acidic vesicles pH (pHav) in both cell lines (Figures 4a and b, white columns). While Baf-A1 treatment increased the vesicular pH and induced cytosolic acidification in both SCR cell lines, the knocking down of TM9SF4 reduced cell sensitivity to Baf-A1-induced pH alterations (Figures 4a and b, gray columns). We also evaluated the process of proton extrusion by a BCECF-based quantification of cultured cell supernatant pH.[26] TM9SF4 knocking down significantly reduces proton accumulation in both cell lines with a consequent increase of extracellular pH (pHe) (Figure 4c). As for intracellular pH, after Baf-A1 treatment extracellular milieu acidification was significantly reduced only in SCR cells (Figure 4c). No differences were observed between SCR and -untransfected cells (not shown).

Taken together, these results indicate that TM9SF4 contributes to V-ATPase-mediated pH regulation, as: (i) TM9SF4 silencing results in pHi acidification, intracellular vesicles alkalization and a reduction of proton accumulation in cell medium; (ii) TM9SF4-knocked down cells are less sensitive to Baf-A1, likely due to a reduction of the amount of its target in an active state. Results and statistical analysis are, respectively, summarized in Table 1 and Supplementary Table S2.

TM9SF4 silencing sensitizes colon cancer cells to 5-FU

An important effect of V-ATPase-mediated pH alterations in cancer cells is the acquirement of a drug-resistant phenotype, as the altered pH gradient decreases intracellular drug accumulation and reduces the binding of the drug to intracellular targets.[9,27] The results obtained in the previous sets of experiments showed a role of TM9SF4 in the maintenance of the reverse pH gradient of colon cancer cells, thus potentially contributing to the pH-mediated chemoresistance.

Following these considerations, we explored TM9SF4 involvement in colon carcinoma cell resistance to 5-FU, the backbone of chemotherapeutic strategies for colorectal carcinoma. SCR and TM9SF4-KD HCT116 and SW480 cells were treated with increasing concentrations of 5-FU (100, 150 and 200 μM) for 48 hours and the effects of TM9SF4 silencing on drug-induced apoptosis and cell growth were assessed. TM9SF4 downregulation significantly increased in both cell lines the effects of 5-FU in terms of cell growth inhibition (Figure 5a) and susceptibility to apoptosis evaluated as the percentage of Annexin-V-positive cells analyzed by fluorescence-assisted cell sorting (FACS) (Figure 5b). TM9SF4 involvement in resistance to 5-FU was further investigated in Hek293T cells (highly sensitive to 5-FU), transfected with a full-length TM9SF4 expression vector to obtain a stable cell line overexpressing TM9SF4 (T-Hek) (Supplementary Figure S1C). T-Hek and mock-transfected cells were treated with different concentrations of 5-FU and cytotoxic effects of 5-FU were analyzed after 24 and 48 h of treatment. TM9SF4 overexpression strongly reduced the sensitivity of T-Hek to 5-FU (Supplementary Figure S3).

To confirm the V-ATPase involvement in TM9SF4-mediated drug resistance, by analogy with experiments described in the previous section, SCR and TM9SF4-KD HCT116 and SW480 cells were respectively pretreated with 10 and 70 nM Baf-A1 for one hour, followed by 100 μM 5-FU for 48 h. In these experiments, summarized in figure 5c, we observed in both cell lines that the Baf-A1 mediated inhibition of V-ATPase increased 5-FU cytotoxic effects exclusively in SCR cells, where the number of apoptotic cells significantly increased, while the number of TM9SF4-KD apoptotic cells was not significantly influenced by the V-ATPase inhibitor. These results suggest that TM9SF4 is a main actor in tumor acidity related drug resistance and also confirm the role of V-ATPase in this phenomenon.

Figure 3. TM9SF4 is involved in V-ATPase assembly. Laser scanning confocal microscopy (LSCM) analysis of TM9SF4 (green) and ATP6V0A2 (red) in (**a**) SCR and (**b**) TM9SF4-KD HCT116 cells. Yellow/orange areas in merged picture indicate colocalization. Scale bar: 10 μm. (**c**) Left panel: Flow cytometry analysis of ATP6V0A2/ATP6V1H association by FRET technique in SCR and TM9SF4-KD HCT116 cells. Numbers indicate the percentage of FL3-positive events obtained in one experiment representative of three. Insets represent ATP6V0A2 intracellular amount in the corresponding sample and is quantitatively expressed by the median fluorescence intensity. Right panel: Bar graph showing the evaluation of FE of ATP6V0A2/ATP6V1H association according to Riemann's algorithm. Results shown represent the mean ± s.d. from three independent experiments. *$P < 0.01$ versus SCR samples. (**d**) Western blot analysis of ATP6V1H immunoprecipitates (IPs) from SCR and TM9SF4-KD HCT116 total lysates immunoblotted with anti-ATP6V0A2. Whole lysates were used as positive controls. In IP lanes, immunoglobulin heavy chains were also detectable. Actin was used as a housekeeping protein. IP0: Immunoprecipitation negative control. (**e**) Densitometric analysis of ATP6V1H, ATP6V0A2 and TM9SF4 proteins in HCT116 cells. Proteins were densitometrically quantified and expressed as percent normalized with β-actin amounts.

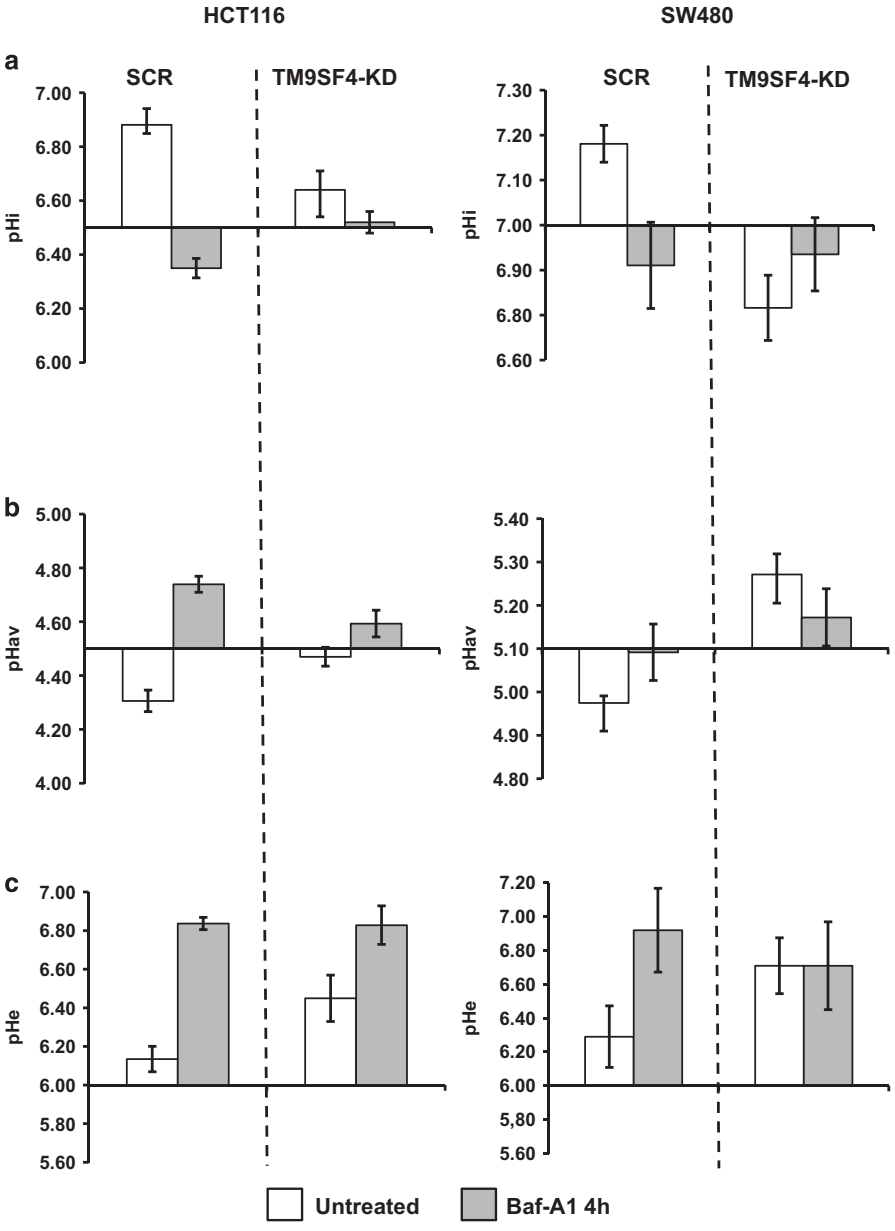

Figure 4. TM9SF4 regulates V-ATPase activity. Spectrofluorimetric pH measurements of untreated (white) and Baf-A1-treated (gray) SCR and TM9SF4-KD HCT116 (right panel) and SW480 (left panel) cell lines. (**a**) BCECF-AM-based pHi measurement; (**b**) pHav measurement of untreated and Baf-A1-treated cells stained with the pH-sensitive probe FITC-dextran. (**c**) BCECF-based pHe measurement values have been obtained using mean fluorescence ratio against a standard curve. $P < 0.05$ versus SCR samples.

TM9SF4 silencing inhibits tumor cell invasiveness

Extracellular acidity increases local invasiveness of cancer cells, and a number of studies have suggested that a key role in cell invasion is played by V-ATPase expressed on the cell surface.[8,28–31] We thus investigated the migration and invasiveness of SCR and TM9SF4-KD cells. Migration was assessed by scratch test and by 8 μm pore size Boyden chamber-based assay, whereas invasiveness was evaluated in an assay based on the utilization of Matrigel-coated Boyden chambers. In chamber-based assays, cells in the lower side of the chamber were stained and analyzed by microscope photography, after removing cells from the upper side of the membrane without (migration assay) or with (invasion assay) Matrigel. While no differences were found in the scratch test and in the migration assay in terms of number and rate of migrated cells at 24, 48 and 72 h (not shown), TM9SF4-KD HCT116 cells showed a strong inhibition of their invasiveness as compared with SCR cells (Figures 6a and b left panel). The number of invading TM9SF4-KD cells decreased by about 82 ± 7% at 24 h and about 69 ± 12% at 48 h as compared with control SCR cells. Similar results were obtained in SCR and TM9SF4-KD SW480 cells (Figure 6b right panel). Finally, experiments to assess the effects of V-ATPase inhibition in the invasive process were also performed using Baf-A1. As expected, the Baf-A1 treatment strongly reduced the number of invading cells in both cell lines (Figure 6c), a result consistent with the literature on V-ATPase involvement in the invasive processes of cancer cells.

Taken together, these results not only indicate that suppression of TM9SF4 inhibits the invasiveness of cancer cells but also confirm a role of V-ATPase in the malignant progression of colon cancer cells.

Table 1. TM9SF4 silencing and pH gradient

	HCT116		*SW480*	
	SCR	*TM9SF4-KD*	*SCR*	*TM9SF4-KD*
pHe				
CTR	6.13 ± 0.066	6.45 ± 0.12	6.29 ± 0.18	6.71 ± 0.16
Baf-A1	6.84 ± 0.032	6.83 ± 0.10	6.92 ± 0.25	6.71 ± 0.26
pHi				
CTR	6.88 ± 0.060	6.64 ± 0.070	7.18 ± 0.041	6,82 ± 0,072
Baf-A1	6.35 ± 0.036	6.52 ± 0.040	6.91 ± 0.096	6.94 ± 0.081
pHav				
CTR	4.31 ± 0.040	4.47 ± 0.052	4.97 ± 0.016	5.27 ± 0.048
Baf-A1	4.74 ± 0.030	4.59 ± 0.063	5.09 ± 0.065	5.17 ± 0.066

Abbreviations: pHav, acidic vesicles pH values obtained with BCECF-AM probe; pHe, extracellular pH values in SCR and TM9SF4-KD HCT116 (left) and SW480 (right) cells obtained with BCECF probe; pHi, cytosolic pH values in the same cells, obtained with FITC-dextran probe. pH differences among pH values in SCR and TM9SF4-KD HCT116 (left) and SW480 (right) cells treated or not, respectively, with 10 and 70 nM Baf-A1 for 4 h. Numbers represent mean ± s.d. of three different experiments.

DISCUSSION

Tumor pH alterations belong to a driver phenotype of malignant cancer cells. These alterations are substantially induced by an aberrant high rate of glycolysis, followed by: (i) lactic acid fermentation in the cytosol; (ii) lactate accumulation in the extracellular spaces and (iii) acidosis, which is increased even more in hypoxic conditions. Tumor cells respond to these 'adverse' conditions avoiding cytosol hyperacidification with a mechanism that is accountable for the reversal of the pH gradient (high pHi versus low pHe). Proteins involved in this process include V-ATPases [14-15], the Na^+/H^+ exchanger 1, Cl^-/HCO_3^- exchangers, Na^+/HCO_3^- cotransporters, H^+/lactate cotransporters (monocarboxylate transporters) and CA II, IX and XII working in a coordinated manner.[15,32,33]

In this study, we have identified TM9SF4 as a new V-ATPase-activating protein that by binding the ATP6V1H subunit of this proton pump, regulates the assembly of the V-ATPase V0/V1 sectors. In our study, we have also observed that TM9SF4 silencing resulted in a series of cellular modifications related with a reduced V-ATPase activity: (i) decrease of pHi; (ii) alkalization of the intracellular vesicles and (iii) alkalization of the extracellular microenvironment through a reduction of protons extrusion. Noteworthy, although tumor cell pH is maintained by an efficient membrane transport machinery including several proteins, it was surprising to observe that the downregulation of TM9SF4 is sufficient to bring back cells to a more physiological pH gradient. Obviously, although in this study we investigated the TM9SF4/V-ATPase association as a key mechanism in tumor pH regulation, a TM9SF4 interaction with other proteins cannot be ruled out. However, our findings suggest a driving role for V-ATPase in this process and more in general in the malignant progression of cancer cells, with TM9SF4 having the role of main character in the V-ATPase-mediated (dis)regulation of tumor pH gradient. This phenomenon is indeed effective on drug resistance, as the excess of protons leads to quick protonation and to the consequent inactivation of the vast majority of the cytotoxic drugs, which do not enter within the target tumor cells or undergo sequestration and inactivation in intracellular vesicles.[9,26,27,34–37] In fact, treatment with proton pump inhibitors not only induces chemosensitizing effects but also are *per se* effective as cytotoxic drugs.[38–40] V-ATPase-mediated proton extrusion is also associated with invasiveness of several tumors, as the acidic extracellular milieu provides the optimal pH for the activation of proteases that digest the extracellular matrix.[41–45]

In this study, consistent with breast and other cancer models,[26,42,46,47] we confirmed that Baf-A1-induced V-ATPase inhibition sensitized to 5-FU and reduced invasiveness of colon cancer cells. More interestingly, we have observed that the knocking down of TM9SF4, inhibiting V-ATPase assembly, sensitized cancer cells to 5-FU (while TM9SF4-overexpressing cells showed clearly a resistant phenotype) and significantly reduced the invasive capacity of the same cells.

Considering that the main mechanism of regulation of V-ATPase activity is the reversible dissociation of the complex into its components (V1 and V0 domains), our results suggest a novel and important new mechanism of V-ATPase regulation controlled by TM9SF4, which has an important role in drug resistance and invasiveness of colon cancer cells.

Based on the results of this study, we hypothesize that in malignant cancer cells TM9SF4 binds to ATP6V1H aberrantly stabilizing the V0/V1 complex; it follows that the proton pump is permanently in an active state, with the consequent acquisition by cancer cells of a more invasive and drug-resistant phenotype (Figure 7).

MATERIALS AND METHODS

Cell cultures

The human colon carcinoma cell lines HCT116 and SW480 were cultured in RPMI 1640 plus 10% fetal calf serum. Hek293T mock and T-Hek cell lines were cultured in high glucose Dulbecco's modified Eagle's medium plus 10% fetal calf serum.

TM9SF4 plasmid construction, transfection and silencing

HCT116 and SW480 cells were transfected with TM9SF4 SureSilencingshRNA plasmid (Qiagen, Venlo, The Netherlands) using Attractene Transfection Reagent (Qiagen) according to the manufacturer's instructions. Scramble SureSilencing shRNA plasmid (Qiagen) was used as a negative control. TM9SF4 downregulation was verified by quantitative PCR.

For construction of the plasmid expressing TM9SF4 protein, the TM9SF4 coding sequence was obtained by PCR amplification using the plasmid pEGFPN1 vector (Clontech, Mountain View, CA, USA) containing the full-length TM9SF4 (GFP-TM9SF4) as the template.[10] Primers used for PCR amplification were as follows: 5′-AAGCTAGCATGTGTGAAACAAGCG-3′ and 5′-AACTCGAGGTCTATCTTCACAGCATA-3′. The TM9SF4 coding sequence was excised with *Nhe*I/*Xho*I and inserted downstream the CMV promoter into the corresponding restriction sites of pTY2CMV-Ires-PuroW. Hek293T cells were transfected with Attractene according to the manufacturer's instructions.

RNA extraction, reverse transcription and quantitative PCR

Total RNA was isolated from cells using Trizol reagent (Invitrogen, Carlsbad, CA, USA). Total RNA was reverse transcribed with High-Capacity cDNA Reverse Transcription Kit (Applied Biosystems, Foster City, CA, USA) according to the manufacturer's instructions. cDNA was subsequently analyzed by quantitative PCR using the TaqMan Universal MasterMix II (Applied Biosystems) and 1× TM9SF4 gene expression assay (Hs00207196_m1) or 1× eukaryotic 18S endogenous control assay (FAM/MGB Probe) (Applied Biosystems). Analysis was performed using the 7500 Software (Applied Biosystems). Template-negative and reverse transcription-negative reactions were used as a negative control. Relative quantification was assessed by $2^{-\Delta\Delta CT}$ calculation using eukaryotic 18S endogenous control as the reference gene.

Laser scanning confocal microscopy

SCR and TM9SF4-KD HCT116 cells were seeded on microscope slide coverslips, fixed with 2% paraformaldehyde and permeabilized with 0.05% Triton X-100. For TM9SF4 and ATP6V0A double staining, cells were labeled with anti-TM9SF4 (Santa Cruz Biotechnology, Santa Cruz, CA, USA) and anti-ATP6V0A2 antibodies (Abcam, Cambridge, UK), respectively, stained with anti-goat Alexa Fluor 488 and anti-rabbit Alexa Fluor 594 (Invitrogen).

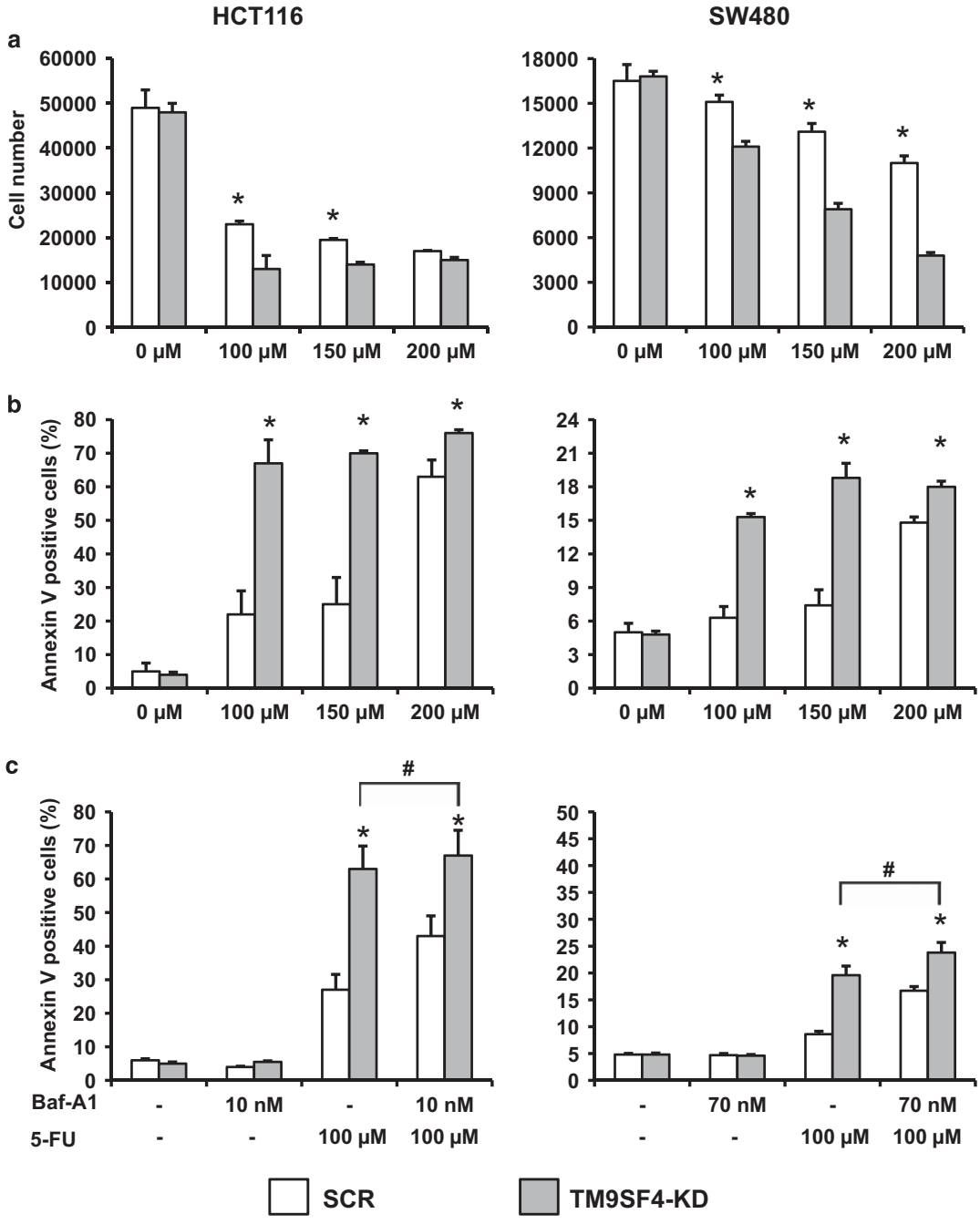

Figure 5. TM9SF4 silencing sensitizes colorectal cancer cells to cytotoxic effects of 5-FU. (**a**) Cell growth of SCR and TM9SF4-KD HCT116 and SW480 cells treated for 48 h with increasing concentration of 5-FU. (**b**) FACS analysis of Annexin-V-positive SCR and TM9SF4-KD HCT116 and SW480 cells treated for 48 h with increasing concentrations of 5-FU. In these experiments, Annexin-V-positive cells were considered apoptotic. (**c**) FACS analysis of Annexin-V-positive SCR and TM9SF4-KD HCT116 and SW480 cells, respectively, pretreated with 10 and 70 nM Baf-A1 for 1 h followed by 100 μM 5-FU for 48 h. In these experiments, Annexin-V-positive cells were considered apoptotic. Results shown represent the mean ± s.d. of the percentage of Annexin-V-positive cells. Each experiment was repeated three times. Differences observed between SCR and TM9SF4-KD cells were statistically significant at all concentrations tested (*$P < 0.05$; #no significant differences). Statistical analysis was performed using analysis of variance one-way Anova and Bonferroni test.

For ATP6V1H and ATP6V0A staining, cells were labeled with anti-ATP6V1H (Santa Cruz Biotechnology) and anti-ATP6V0A2 (Abcam), respectively, stained with anti-mouse Alexa Fluor 488 and anti-rabbit Alexa Fluor 594. Observations were performed using a Leica TCS SP2 spectral confocal microscopy (Leica Microsystems, Heidelberg, Germany) equipped with argon-helium neon (Ar-HeNe) lasers. The excitation wavelength used was 488 nm for indirect staining of TM9SF4 and ATP6V1H; the excitation wavelength used was 543 nm to evaluate ATP6V0A. Emission lines were collected after passage through a double dichroic filter (DD488/543) in a spectral window ranging from 580 to 783 nm. Spectral window ranges used for each protein were as follows: TM9SF4: 501–540 nm; ATP6V1H: 558–710 nm; and ATP6V0A: 565–710 nm. Acquisition parameters used were as follows: 63.0/1.4 NA HCXPLAPOCS objective; image size: 1024 × 1024; pinhole size: 1 Airy; and scan mode xyz, step size: 0.5 μm. Images were processed using the LCS (Leica Microsystems) software program.

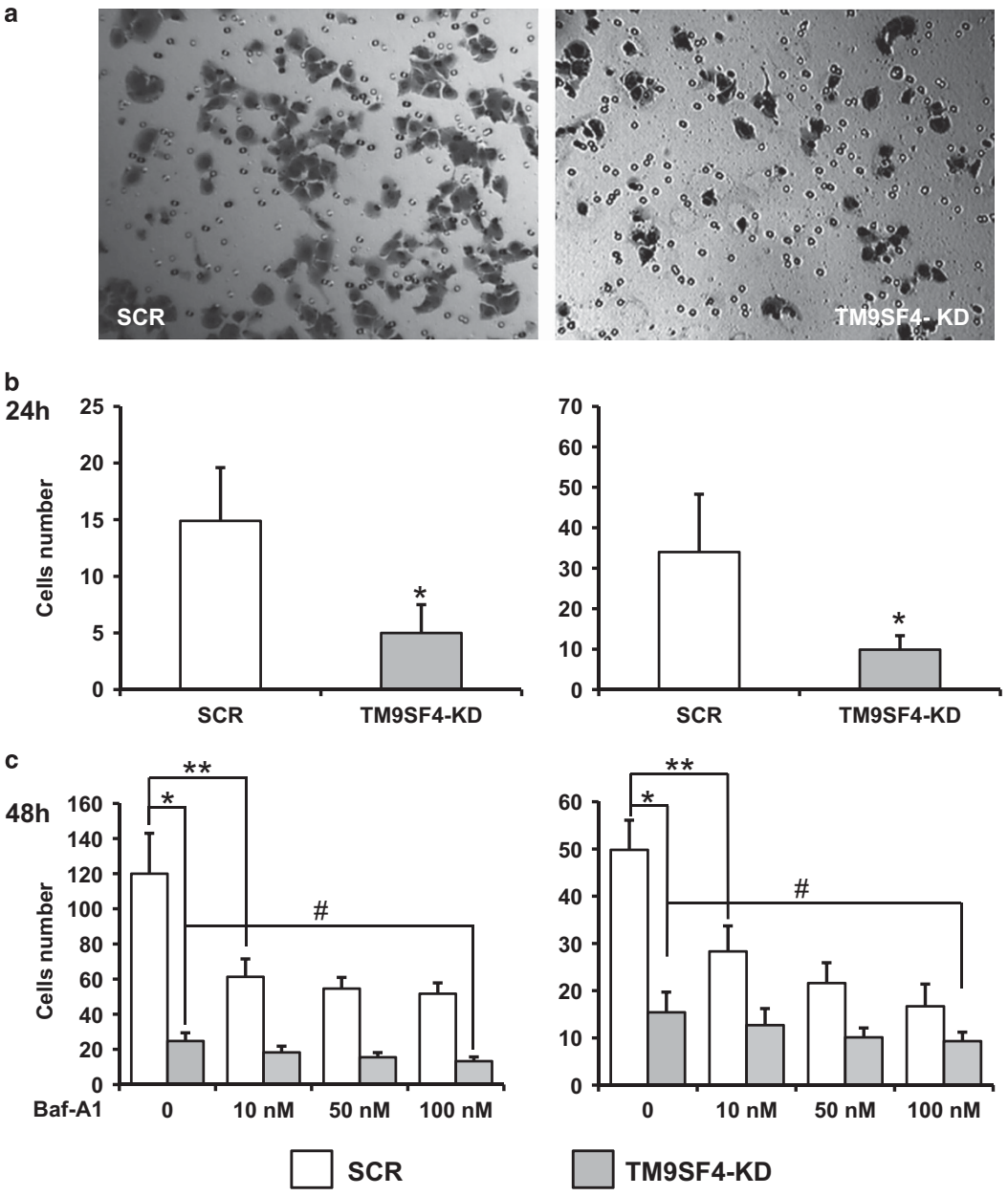

Figure 6. TM9SF4 silencing inhibits tumor cells invasiveness. (**a**) Micrographs of crystal violet-stained invading SCR (left) and TM9SF4-KD (right) HCT116 cells in the lower side of a Boyden chamber with 8 μm pore size polycarbonate membrane coated with Matrigel after 48 h of seeding. (**b**) Bar graph showing the number of invading SCR and TM9SF4-KD HCT116 (left) and SW480 (right) cells after 24 h of seeding. (**c**) Bar graph representing the number of invading SCR and TM9SF4-KD cells treated with increasing concentrations of Baf-A1 for 48 h after seeding. Data are expressed as mean ± s.d. of values obtained in three different experiments performed in triplicate. (*$P < 0.05$; **$P < 0.01$; #no statistically significant differences)

pHav measurement

pHav was measured by fluorimetric analysis of cells loaded with FITC-dextran, modifying the protocol described in Ohkuma and Poole.[48] Briefly, SCR and TM9SF4-KD HCT116 cells were seeded in a 96 Nunc-Immuno MicroWell plate (Sigma-Aldrich, St Louis, MO, USA), and after 24 h, the growth medium was replaced by the same medium buffered with phosphate buffer (KH_2PO_4/K_2HPO_4 molar ratio: 1:1, 2g/l, pH 7.4) for 24 h with or without 10 nM Baf-A1 (Sigma-Aldrich) in the last 4 h. After 4 h, FITC-dextran (MW 40 000; Sigma-Aldrich) was added for 30 min to a final concentration of 1 mg/ml. Fluorescence intensity was measured with a fluorometer Perkin-Elmer LS-50B setting the instrument at the following wavelengths: 440–490 nm for excitation and 525 nm for emission. Calibration curve was created using the high K^+/Nigericin solution in a range of pH (4.0–5.5).[49] High K^+/Nigericin solution included 10 μM Nigericin (Sigma-Aldrich), 136 mm KCl, 1 mM KH_2PO_4, 0.5 mM $CaCl_2$, 10 mM HEPES and 5 mM d-glucose.

Evaluation of pHi

pHi was measured in cells loaded with the fluorescent probe BCECF-AM according to Seo *et al.*[50] Briefly, after Baf-A1 treatment as described above, BCECF-AM (Invitrogen) was added for 30 min to a final concentration of 1 μM. Fluorescence intensity was measured as described above. Calibration curve was created using the high K^+/Nigericin solution in a range of pH (5.0–7.2).[51]

Extracellular pH

pHe was calculated according to Lu *et al.*[45] Briefly, SCR and TM9SF4-KD HCT116 and SW480 cells were seeded as described above in RPMI 1640 with or without HCO_3, which was buffered with phosphate buffer (KH_2PO_4/K_2HPO_4 molar ratio: 1:1, 2 g/l, pH 7.4) with or without Baf-A1. At the end of Baf-A1 treatment, 100 μl of growth medium were transferred into a

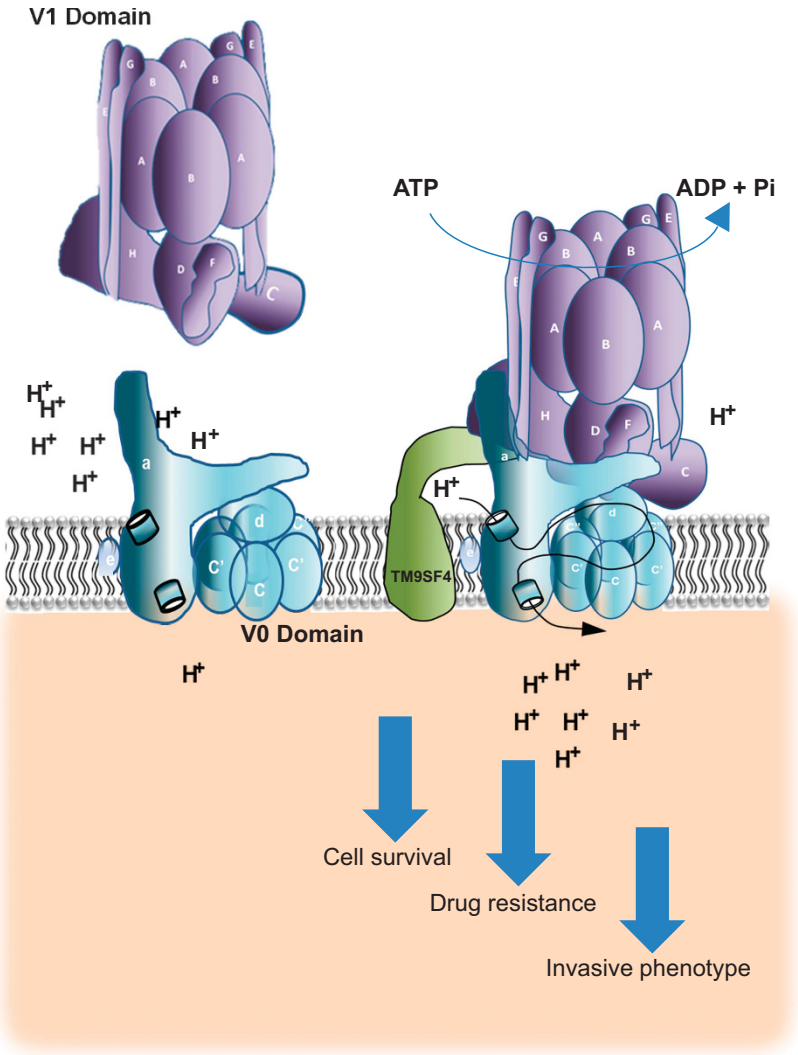

Figure 7. Hypothetic model of protein–protein interaction between V-ATPase and TM9SF4 in colon cancer cells. TM9SF4 interacting with ATP6V1H promotes interaction of ATP6V0A with ATP6V1H subunit of V-ATPase. These biochemical events are important for V-ATPase activities. Inhibition of TM9SF4 impairs the interaction of V-ATPase V0/V1 sections resulting in: (i) extracellular and vesicle alkalization and (ii) cytosol pH decrease.

96 Nunc-Immuno MicroWell plate and 1 μM BCECF (final concentration) was added for 30 min in each well. Fluorescence intensity was measured with Perkin-Elmer LS-50B setting the instrument at the following wavelengths: 440–490 nm for excitation and at 525 nm for emission. Standard curve was obtained by adding BCECF (Invitrogen) in RPMI 1640 plus 10% fetal calf serum, which was buffered at various pH (6.0–7.2) with phosphate buffer.

All pH values were calculated using 490/440 nm fluorescence ratio and using the standard curve and linear equations shown in Supplementary Figure S4.

Immunoprecipitation and western blotting

Immunoprecipitation and western blotting were carried out following standard protocols, using the anti-ATP6V1H clone G-2 mAb (Santa Cruz Biotechnology) as an immunoprecipitating antibody. Sodium dodecyl sulfate–polyacrylamide gel electrophoresis and western blotting were carried out following the standard protocols. For immunoblotting, the following antibodies were used: anti-TM9SF4 polyclonal antibody (Novus Biological, Littleton, CO, USA); anti-ATP6VOA2 polyclonal antibody (Abcam); anti-ATP6V1H (Santa Cruz Biotechnology); and anti-β-actin (Sigma-Aldrich). As secondary antibodies, appropriate horseradish peroxidase-conjugated antibodies (GE Healthcare, Amersham, UK) were used. Densitometry was carried out using Image J software (v1.46 d, GE Healthcare).

Fluorescence resonance energy transfer

We applied FRET analysis[52] by flow cytometry to study the molecular association of: (i) TM9SF4/ATP6V1H, (ii) ATP6V1H/ATP6V0A (positive control) and (iii) TM9SF4/LAMP1 (negative control). Briefly, cells were fixed and permeabilized as above, washed two times in cold phosphate-buffered saline and then labeled with antibodies tagged with donor (PE) or acceptor (Cy5) dyes. TM9SF4 staining was performed using a polyclonal rabbit antibody (Novus Biological); for ATP6V1H and ATP6V0A, a monoclonal mouse antibody (Santa Cruz Biotechnology) and a rabbit polyclonal antibody (Abcam) were, respectively, used. As secondary antibodies, biotinylated anti-mouse IgG1 followed by saturating concentrations of streptavidin-Cy5 (both from BD Pharmingen, Franklin Lakes, NJ, USA) or anti-rabbit-PE (BD Pharmingen) were used. After staining, cells were washed two times, resuspended in phosphate-buffered saline and analyzed with a dual-laser FACScalibur flow cytometer (BD Biosciences, Heidelberg, Germany). For determination of FE, changes in fluorescence intensities of donor plus acceptor-labeled cells were compared with the emission signal from cells labeled with donor- and acceptor-only fluorophores. All data were corrected for background by subtracting the binding of the isotype controls. Efficient energy transfer resulted in an increased acceptor emission on cells stained with both donor and acceptor dyes. The FE was calculated according to Riemann *et al.*[52] For details see the Supplementary Data.

In vitro growth inhibition and apoptosis

SCR and TM9SF4-KD HCT116 and SW480 colon carcinoma cells were seeded in 24 multiwells and preincubated overnight. After changing the medium, cells were treated with different concentrations of 5-FU (100–150–200 μM). After exposure for 48 or 72 h, the whole-cell amount of each well was stained with 1 μl Annexin-V and 1 μl propidium iodide (eBioscience Kit, San Diego, CA, USA). Samples were analyzed by FACS to assess the percentage of apoptosis (Annexin-V positive) or necrosis (propidium iodide-positive cells). For flow cytometry studies, all samples were analyzed by a dual-laser FACScalibur cytometer (BD Biosciences) equipped with a 488 nm argon laser. Data were recorded and statistically analyzed by a Macintosh computer using Cell Quest Pro software (BD Biosciences).

Migration and invasion test

The ability of cells to migrate through filters was measured using Polycarbonate Membrane Transwell Inserts (Corning Inc., Corning, NY, USA). Cell culture inserts with an 8 μm pore size polycarbonate membrane were used according to the manufacturer's protocol. The bottom chamber included medium (0.5 ml) containing 10% fetal bovine serum. SCR and TM9SF4-KD HCT116 and SW480 cells were seeded in 0.5 ml of medium with or without fetal bovine serum into the upper chamber and incubated at 37 °C in a humidified atmosphere containing 5% CO_2. After 24 and 48 h, cells on the upper surface were mechanically removed with a cotton swab, membranes were then washed, fixed and stained using crystal violet (Sigma-Aldrich). The migration ability of the cells was determined by counting the cells that had migrated to the lower side of the membrane with a microscope.

For the Matrigel-coated transwell assay (Invasion test), the same procedures described above were used, seeding cells in the upper chamber of Matrigel-coated 8 μm pore size transwells (BD Biosciences) in serum-free medium, whereas HCT116 or SW480 cell conditioned medium was used as the chemotactic factor in the inferior room of the Boyden chamber. The invasive ability of the cells was determined 24 and 48 h after seeding.

All experiments were performed in triplicate. In each experiment at least three fields were counted.

Data analysis

All data reported in this paper were verified in at least three different experiments and reported as mean ± s.d., if not differently specified. Statistical analysis between different experimental conditions was performed with the analysis of variance test, followed by the Bonferroni comparison of means (when appropriate), using the GraphPad software (La Jolla, CA, USA). $P \leqslant 0.05$ indicates the statistical significance.

CONFLICT OF INTEREST

The authors declare no conflict of interest.

ACKNOWLEDGEMENTS

We thank Dr Angelo De Milito for helpful discussion, Pasqualina Leone for her contribution in plasmid cloning and Dr Tonino Sofia for his suggestions. This study was supported by AIRC Associazione Italiana per la Ricerca sul Cancro. Airc Grant '10602' and 'IG 11505n'. The funders had no role in study design, data collection and analysis, decision to publish or preparation of the manuscript.

AUTHOR CONTRIBUTIONS

FL conceived the study, designed and supervised the experiments; MB, FM, GV, SF and AC provided critical advice and contributed to manuscript revisions; MB, FM, EI, TA, PM, SM and RM performed experiments; AC performed quantitative reverse transcription–PCR experiments; TA performed statistical analyses; and FL wrote the manuscript.

REFERENCES

1 De Souza AC, Justo GZ, de Araújo DR, Cavagis AD. Defining the molecular basis of tumor metabolism: a continuing challenge since Warburg's discovery. *Cell Physiol Biochem* 2011; **28**: 771–792.
2 De Milito A, Marino ML, Fais S. A rationale for the use of proton pump inhibitors as antineoplastic agents. *Curr Pharm Des* 2012; **18**: 1395–1406.
3 Zhang Y, Yang JM. Altered energy metabolism in cancer: a unique opportunity for therapeutic intervention. *Cancer Biol Ther* 2013; **14**: 81–89.
4 Simon S, Roy D, Schindler M. Intracellular pH and the control of multidrug resistance. *Proc Natl Acad Sci USA* 1994; **91**: 1128–1132.
5 Raghunand N, Gillies RJ. pH and drug resistance in tumors. *Drug Resist Updat* 2000; **3**: 39–47.
6 Rofstad EK, Mathiesen B, Kindem K, Galappathi K. Acidic extracellular pH promotes experimental metastasis of human melanoma cells in athymic nude mice. *Cancer Res* 2006; **66**: 6699–6707.
7 Fais S, De Milito A, You H, Qin W. Targeting vacuolar H+-ATPases as a new strategy against cancer. *Cancer Res* 2007; **67**: 10627–10630.
8 Estrella V, Chen T, Lloyd M, Wojtkowiak J, Cornnell HH, Ibrahim-Hashim A *et al.* Acidity generated by the tumor microenvironment drives local invasion. *Cancer Res* 2013; **73**: 1524–1535.
9 Daniel C, Bell C, Burton C, Harguindey S, Reshkin SJ, Rauch C. The role of proton dynamics in the development and maintenance of multidrug resistance in cancer. *Biochim Biophys Acta* 2013; **1832**: 606–617.
10 Nishi T, Forgac M. The vacuolar (H+)-ATPases-nature's most versatile proton pumps. *Nat Rev Mol Cell Biol* 2002; **3**: 94–103.
11 Hurtado-Lorenzo A, Skinner M, El Annan J, Futai M, Sun-Wada GH, Bourgoin S *et al.* V-ATPase interacts with ARNO and Arf6 in early endosomes and regulates the protein degradative pathway. *Nat Cell Biol* 2006; **8**: 124–136.
12 Qi J, Wang Y, Forgac M. The vacuolar (H+)-ATPase: subunit arrangement and *in vivo* regulation. *J Bioenerg Biomembr* 2007; **39**: 423–426.
13 Marshansky V, Rubinstein JL, Grüber G. Eukaryotic V-ATPase: novel structural findings and functional insights. *Biochim Biophys Acta* 2014; **1837**: 857–879.
14 Sun-Wada GH, Wada Y. Vacuolar-type proton pump ATPases: acidification and pathological relationships. *Histol Histopathol* 2013; **28**: 805–815.
15 Fogarty FM, O'Keeffe J, Zhadanov A, Papkovsky D, Ayllon V, O'Connor R. HRG-1 enhances cancer cell invasive potential and couples glucose metabolism to cytosolic/extracellular pH gradient regulation by the vacuolar-H(+) ATPase. *Oncogene* 2014; **33**: 4653–4663.
16 Sennoune SR, Bakunts K, Martínez GM, Chua-Tuan JL, Kebir Y, Attaya MN *et al.* Vacuolar H+-ATPase in human breast cancer cells with distinct metastatic potential: distribution and functional activity. *Am J Physiol Cell Physiol* 2004; **286**: C1443–C1452.
17 Supino R, Scovassi AI, Croce AC, Dal Bo L, Favini E, Corbelli A *et al.* Biological effects of a new vacuolar-H,-ATPase inhibitor in colon carcinoma cell lines. *Ann NY Acad Sci* 2009; **1171**: 606–616.
18 Perrin J, Mortier M, Jacomin AC, Viargues P, Thevenon D, Fauvarque MO. The Nonaspanins TM9SF2 and TM9SF4 regulate the plasma membrane localization and signalling activity of the peptidoglycan recognition protein PGRP-LC in *Drosophila*. *J Innate Immun* 2014; **7**: 37–46.
19 He P, Peng Z, Luo Y, Wang L, Yu P, Deng W *et al.* High-throughput functional screening for autophagy-related genes and identification of TM9SF1 as an autophagosome-inducing gene. *Autophagy* 2009; **5**: 52–60.
20 Zaravinos A, Lambrou GI, Boulalas I, Delakas D, Spandidos DA. Identification of common differentially expressed genes in urinary bladder cancer. *PLoS One* 2011; **6**: e18135.
21 Chang H, Jeung HC, Jung JJ, Kim TS, Rha SY, Chung HC. Identification of genes associated with chemosensitivity to SAHA/taxane combination treatment in taxane-resistant breast cancer cells. *Breast Cancer Res Treat* 2011; **125**: 55–63.
22 Oo HZ, Sentani K, Sakamoto N, Anami K, Naito Y, Oshima T *et al.* Identification of novel transmembrane proteins in scirrhous-type gastric cancer by the *Escherichia coli* ampicillin secretion trap (CAST) method: TM9SF3 participates in tumor invasion and serves as a prognostic factor. *Pathobiology* 2014; **81**: 138–148.
23 Lozupone F, Perdicchio M, Brambilla D, Borghi M, Meschini S, Barca S *et al.* The human homologue of Dictyosteliumdiscoideum phg1A is expressed by human metastatic melanoma cells. *EMBO Rep* 2009; **10**: 1348–1354.
24 Mackinnon RN, Selan C, Wall M, Baker E, Nandurkar H, Campbell LJ. The paradox of 20q11.21 amplification in a subset of cases of myeloid malignancy with chromosome 20 deletion. *Genes Chromosomes Cancer* 2010; **49**: 998–1013.
25 von Heijne G. Membrane protein structure prediction, hydrophobicity analysis and the positive-inside rule. *J MolBiol* 1992; **225**: 487–494.
26 Chen M, Huang SL, Zhang XQ, Zhang B, Zhu H, Yang VW *et al.* Reversal effects of pantoprazole on multidrug resistance in human gastric adenocarcinoma cells by down-regulating the V-ATPases/mTOR/HIF-1α/P-gp and MRP1 signaling pathway *in vitro* and *in vivo*. *J Cell Biochem* 2012; **113**: 2474–2487.
27 Pérez-Sayáns M, Somoza-Martín JM, Barros-Angueira F, Diz PG, Rey JM, García-García A. Multidrug resistance in oral squamous cell carcinoma: the role of vacuolar ATPases. *Cancer Lett* 2010; **295**: 135–143.
28 Michel V, Licon-Munoz Y, Trujillo K, Bisoffi M, Parra KJ. Inhibitors of vacuolar ATPase proton pumps inhibit human prostate cancer cell invasion and prostate-specific antigen expression and secretion. *Int J Cancer* 2013; **132**: E1–10.

29 Graham RM, Thompson JW, Webster KA. Inhibition of the vacuolar ATPase induces Bnip3-dependent death of cancer cells and a reduction in tumor burden and metastasis. *Oncotarget* 2014; **5**: 1162–1173.
30 Wiedmann RM, von Schwarzenberg K, Palamidessi A, Schreiner L, Kubisch R, Liebl J *et al.* The V-ATPase-inhibitor archazolid abrogates tumor metastasis via inhibition of endocytic activation of the Rho-GTPase Rac1. *Cancer Res* 2012; **72**: 5976–5987.
31 Capecci J, Forgac M. The function of vacuolar ATPase (V-ATPase) a subunit isoforms in invasiveness of MCF10a and MCF10CA1a human breast cancer cells. *J Biol Chem* 2013; **288**: 32731–32741.
32 Parks SK, Chiche J, Pouysségur J. Disrupting proton dynamics and energy metabolism for cancer therapy. *Nat Rev Cancer* 2013; **9**: 611–623.
33 Parks SK, Chiche J, Pouyssegur J. pH control mechanisms of tumor survival and growth. *J Cell Physiol* 2011; **226**: 299–308.
34 Murakami T, Shibuya I, Ise T, Chen ZS, Akiyama S, Nakagawa M *et al.* Elevated expression of vacuolar proton pump genes and cellular pH in cisplatin resistance. *Int J Cancer* 2001; **93**: 869–874.
35 Niikura K. Vacuolar ATPase as a drug discovery target. *Drug News Perspect* 2006; **19**: 139–144.
36 De Milito A, Fais S. Tumor acidity, chemoresistance and proton pump inhibitors. *Fut Oncol* 2005; **1**: 779–786.
37 You H, Jin J, Shu H, Yu B, De Milito A, Lozupone F *et al.* Small interfering RNA targeting the subunit ATP6L of proton pump V-ATPase overcomes chemoresistance of breast cancer cells. *Cancer Lett* 2009; **280**: 110–119.
38 Luciani F, Spada M, De Milito A, Molinari A, Rivoltini L, Montinaro A *et al.* Effect of proton pump inhibitor pretreatment on resistance of solid tumors to cytotoxic drugs. *J Natl Cancer Inst* 2004; **96**: 1702–1713.
39 De Milito A, Canese R, Marino ML, Borghi M, Iero M, Villa A *et al.* pH-dependent antitumor activity of proton pump inhibitors against human melanoma is mediated by inhibition of tumor acidity. *Int J Cancer* 2010; **127**: 207–219.
40 Spugnini EP, Baldi A, Buglioni S, Carocci F, de Bazzichini GM, Betti G *et al.* Lansoprazole as a rescue agent in chemoresistant tumors: a phase I/II study in companion animals with spontaneously occurring tumors. *J Transl Med* 2011; **9**: 221.
41 Gocheva V, Joyce JA. Cysteine cathepsins and the cutting edge of cancer invasion. *Cell Cycle* 2007; **6**: 60–64.
42 Hinton A, Sennoune SR, Bond S, Fang M, Reuveni M, Sahagian GG *et al.* Function of a subunit isoforms of the V-ATPase in pH homeostasis and *in vitro* invasion of MDA-MB231 human breast cancer cells. *J Biol Chem* 2009; **284**: 16400–16408.
43 Chung C, Mader CC, Schmitz JC, Atladottir J, Fitchev P, Cornwell ML *et al.* The vacuolar-ATPase modulates matrix metalloproteinase isoforms in human pancreatic cancer. *Lab Invest* 2011; **91**: 732–743.
44 Nishisho T, Hata K, Nakanishi M, Morita Y, Sun-Wada GH, Wada Y *et al.* The a3 isoform vacuolar type H^+-ATPase promotes distant metastasis in the mouse B16 melanoma cells. *Mol Cancer Res* 2011; **9**: 845–855.
45 Lu X, Qin W, Li J, Tan N, Pan D, Zhang H *et al.* The growth and metastasis of human hepatocellular carcinoma xenografts are inhibited by small interfering RNA targeting to the subunit ATP6L of proton pump. *Cancer Res* 2005; **65**: 6843–6849.
46 Avnet S, Di Pompo G, Lemma S, Salerno M, Perut F, Bonuccelli G. V-ATPase is a candidate therapeutic target for Ewing sarcoma. *Biochim Biophys Acta* 2013; **18328**: 1105–1116.
47 Xu J, Xie R, Liu X, Wen G, Jin H, Yu Z *et al.* Expression and functional role of vacuolar H(+)-ATPase in human hepatocellular carcinoma. *Carcinogenesis* 2012; **33**: 2432–2440.
48 Ohkuma S, Poole B. Fluorescence probe measurement of the intralysosomal pH in living cells and the perturbation of pH by various agents. *Proc Natl Acad Sci USA* 1978; **75**: 3327–3331.
49 Thomas JA, Buchsbaum RN, Zimniak A, Racker E. Intracellular pH measurements in Ehrlich ascites tumor cells utilizing spectroscopic probes generated *in situ*. *Biochemistry* 1979; **18**: 2210–2218.
50 Seo JT, Steward MC, Larcombe-McDouall JB, Cook LJ, Case RM. Continuous fluorometric measurement of intracellular pH and Ca^{2+} in perfused salivary gland and pancreas. *Pflugers Arch* 1994; **426**: 75–82.
51 Stryer L. Fluorescence energy transfer as a spectroscopic ruler. *Annu Rev Biochem* 1978; **47**: 819–846.
52 Riemann D, Tcherkes A, Hansen GH, Wulfaenger J, Blosz T, Danielsen EM. Functional co-localization of monocyticaminopeptidase N/CD13 with the Fc gamma receptors CD32 and CD64. *Biochem Biophys Res Commun* 2005; **331**: 1408–1412.

Supplementary Information accompanies this paper on the Oncogene website (http://www.nature.com/onc)